Optical evidence for substrate-induced growth of ultrathin hexa-*peri*-hexabenzocoronene films on highly oriented pyrolytic graphite

Roman Forker, Thomas Dienel, and Torsten Fritz*
Institut für Angewandte Photophysik, TU Dresden, D-01062 Dresden, Germany

Klaus Müllen
Max-Planck-Institut für Polymerforschung, Ackermannweg 10, D-55172 Mainz, Germany
(Received 27 January 2006; revised manuscript received 18 May 2006; published 23 October 2006)

We describe the influence of the substrate on the optical properties of ultrathin hexa-*peri*-hexabenzocoronene (HBC) layers deposited by organic molecular beam epitaxy. For that purpose, *in situ* differential reflectance spectroscopy (DRS) was employed, providing unsurpassed sensitivity for the thickness-dependent optical analysis. From the DR spectra, the optical functions were extracted using a numerical algorithm. The obtained spectra vary significantly for different substrates. We interpret these variances as being due to the different growth modes of HBC films altered by the influence of the respective substrate. HBC shows polycrystalline island structures on fused quartz in atomic force microscopy. On the other hand, layer-by-layer growth along with the formation of quasi-one-dimensional stacks on highly oriented pyrolytic graphite is known from previously published structural examinations. In this contribution, the optically observed monomer→dimer →oligomer transition, indicated by the occurrence of isosbestic points, is related to the findings for perylene-tetracarboxylic dianhydride layers on mica.

DOI: 10.1103/PhysRevB.74.165410 PACS number(s): 78.66.Qn, 78.20.Ci, 78.40.Me

I. INTRODUCTION

Organic thin films are nowadays widely used in various electronic devices, such as organic solar cells and OLEDs.[1,2] More sophisticated miniaturized applications will require well-defined interfaces with conductive contacts and the control of the film structure at a molecular level. For that purpose, it is indispensable to aim at a thickness-dependent characterization of the physical properties, preferably during film growth. A nondestructive method with high accuracy suitable for this task is provided by the differential reflectance spectroscopy (DRS).[3,4] With this technique, remarkable insight in the optical properties of ultrathin films of 3,4,9,10-perylenetetracarboxylic dianhydride (PTCDA, $C_{24}H_8O_6$, Fig. 1) was attained.[5,6] Thickness-dependent optical phenomena, such as the monomer→dimer transition, could readily be explained in terms of excitonic processes which occur in a quasi-one-dimensional crystal.[7–9] Furthermore, the very sensitive dependence of the optical functions on the modification of the crystal structure (e.g., α- and β-phase for PTCDA[10]) was proven by DRS.[11]

Based on these findings for PTCDA, we were driven by the question how the optical behavior of materials *not* exhibiting a crystal structure with one-dimensional character would look like. Can we generally find evidence for the monomer→dimer transition? Are there any examples for substrate-induced growth altering the character of the crystal structure and thus the optical properties? To clarify these questions, we performed DRS measurements on substrates of different nature, namely highly oriented pyrolytic graphite (HOPG) and fused quartz. The molecule we report on here is hexa-*peri*-hexabenzocoronene (HBC, $C_{42}H_{18}$, Fig. 1), a disklike polycyclic aromatic hydrocarbon (PAH) of D_{6h} symmetry. The optical properties of HBC monomers are known from absorbance measurements in solution.[12] Substituting short side chains on the outermost carbon atoms of its aromatic framework yields only very small deviations from the optical transitions of the isolated molecule, even for a large variety of substituents.[13–18] However, because of steric reasons, the side chains do affect the packing properties of bulk structures. The HBC derivatives presented in Ref. 14 self-assemble into columnar stacks. This becomes manifest in an altered absorbance spectrum for alkyl-substituted HBC aggregates (cf. Fig. 2). Close resemblances to the optical spectra of (unsubstituted) HBC layers on HOPG are reported in this paper. Further similarities to the optical behavior of columnar PTCDA-crystals are demonstrated, namely the visibility of the monomer→dimer transition indicated by isosbestic points. We will provide evidence that HBC grows in different crystal polymorphs on HOPG and on fused quartz, adopting a stacked molecular alignment on HOPG due to substrate-induced growth.

This paper is divided into three parts: First, we give a brief overview over the principle of the DRS measurement and we summarize a recently developed algorithm[11] needed to extract the optical functions from the DRS. Second, we discuss the obtained optical functions and compare them to *ex situ* absorbance measurements of HBC aggregates with different structures on different substrates. Finally, we address the issue of the oscillator strength by means of the so-called effective medium approximation (EMA).

II. MEASUREMENT PRINCIPLE

A. Differential reflectance spectroscopy

Structural investigations of molecular layers are commonly done by STM or LEED measurements. This requires the use of conductive substrates, such as graphite or metals. For opaque substrates, the reflectance is the only accessible

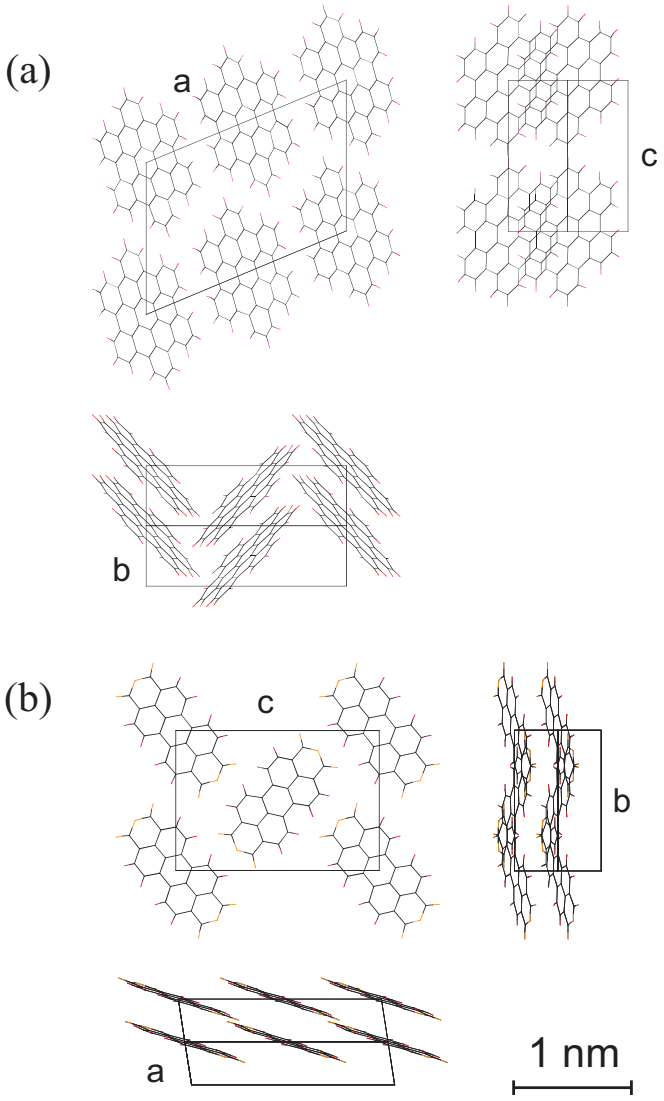

FIG. 1. (Color online) (a) Arrangement of the molecules in the HBC bulk crystal. HBC is "fully benzenoid" and has therefore an extended π electron system. There is no crystal plane with flat lying molecules (Ref. 19). (b) Arrangement of the molecules in the α-PTCDA bulk crystal. Note that the in-plane separation is much higher than the distance of two adjacent molecules in the stacking direction. The aromaticity of the benzenoid frameworks is not explicitly indicated (Ref. 20).

optical quantity. With the optical setup described in Ref. 6, it is feasible to record differential reflectance spectra *in situ*, i.e., during the deposition of the molecules. It is therefore possible to study thickness-dependent optical quantities and to monitor the growth of molecular layers. The simple definition of the DRS

$$\mathrm{DRS} \equiv \frac{\Delta R}{R}(\omega,d) := \frac{R(\omega,d) - R_0(\omega)}{R_0(\omega)} \tag{1}$$

can be interpreted as a change in the reflectance from the bare substrate $R_0(\omega)$ to that of the substrate with a deposited film $R(\omega)$, normalized by $R_0(\omega)$. Following the proposal in Ref. 3, the complex Fresnel equations of the two-interface

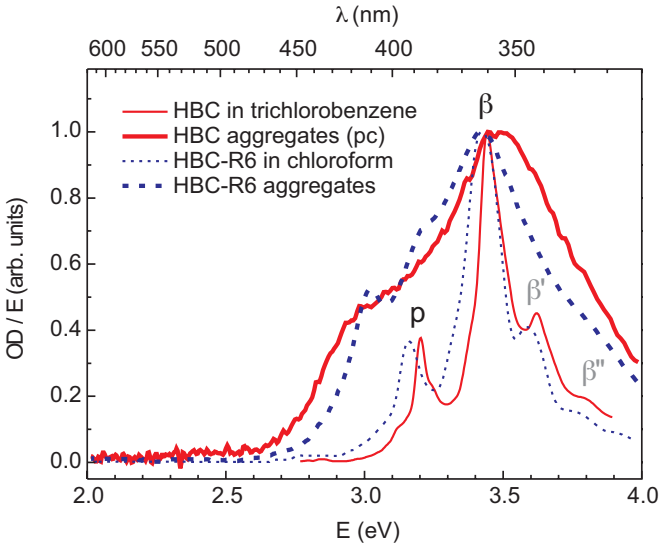

FIG. 2. (Color online) Normalized *ex situ* absorbance of HBC (Refs. 12 and 21) (solid lines) and alkyl-substituted HBC (Ref. 14) (HBC-R6, dashed lines) in solution and as aggregates on fused quartz. Monomer-peaks of isolated molecules (in solution) are named in the Clar nomenclature (Ref. 22). Note that the solution spectra are almost identical except for the different solvent shifts.

system (void–thin film–substrate) can be linearized for ultrathin films (thickness $\ll$ wavelength of incident light). It has been shown that in the case of normal incidence (nearly fulfilled here) and transparent substrates, the DRS is essentially proportional to the absorbance of the deposited film:[3,6]

$$\mathrm{DRS} \approx -\frac{8\pi d}{\lambda}\frac{\varepsilon''}{1-\varepsilon_{\mathrm{substrate}}}, \tag{2}$$

with d being the film thickness, $\hat{\varepsilon}=\varepsilon'-i\varepsilon''$ the complex dielectric function of the film, and $\varepsilon_{\mathrm{substrate}}$ the real part of the substrate's dielectric function (its imaginary part is negligible in this approximation). For opaque substrates, however, no such general equivalence can be established. For this reason, it is indispensable to extract the optical functions $n(\omega)$ and $k(\omega)$ of the molecular film. This permits a comparison between the optical properties of films of a given molecular species on different substrates.

B. Determination of optical functions

In this section, we summarize the fundamentals of a recently developed algorithm,[11] designed to extract the *two* optical functions n and k from spectral measurements. The principal difficulty of this task is that we only have *one* quantity which can be measured, namely the DRS. An apparently simple way to solve this problem is the fact that n and k are related to each other via the Kramers-Kronig transformation[23,24]

$$n(E_i) = n(\infty) + \frac{2}{\pi}\mathcal{P}\int_0^\infty \frac{k(E)E}{E^2 - E_i^2}dE, \tag{3}$$

where $\mathcal{P}$ symbolizes the Cauchy principal value of the integral. The number $n(\infty)$ is the high energy offset of the

n-spectrum in the case of an integral over the entire energy range. As it is obviously only possible to record spectra over a finite energy range, one has to divide this integral into a sum of three integrals, one of which covers the measurable range $[E_L, E_U]$. The mathematical rearrangement shown in Ref. 11 leads to the expression

$$n(E_i) = n_{\text{offset}} + \frac{2}{\pi}\mathcal{P}\int_{E_L}^{E_U} \frac{k(E)E}{E^2 - E_i^2} dE,$$

$$E_L \leqslant E_i \leqslant E_U, \tag{4}$$

where n_{offset} is treated as a fit parameter by the algorithm.

The "heart" of the utilized algorithm consists of a variation of the k-spectrum with a subsequent calculation of the corresponding n-spectrum by means of Eq. (4). These n- and k-spectra are the basis of computing the differential reflectance signal using the exact thin film optics formulas for a homogeneous thin film with plane and parallel boundaries on an optically thick substrate. This further requires the knowledge of the film thickness and of the optical functions of the substrate. The difference between the computed and the measured DRS is minimized iteratively:

$$[\text{DRS}_{\text{experiment}}(E_i) - \text{DRS}_{\text{calculation}}(n(E_i), k(E_i))]^2 \rightarrow \text{minimum}. \tag{5}$$

The best set of optical functions $n(E_i)$ and $k(E_i)$ fulfilling the condition (5) is the result of the numerical fit procedure. A far more detailed description of this model-free algorithm is given in Ref. 11. There, the authors take great care to explain the constraints of this method and the problems that arise from the finite energy range of the accessible spectrum. They also focus on ways to overcome these difficulties, e.g., by extrapolation procedures and by exploiting the phase information. The algorithm was tested on both analytically generated and experimental spectra, and has proven to yield highly accurate results.[25,26]

Although the conversion between $\hat{\varepsilon}$ and $\hat{n}$ is rather simple,[27] those two quantities are not quite identical. While *reflection* and *refraction* are commonly expressed in terms of $\hat{n}(\omega)$, the material's *absorption* behavior should be described by $\hat{\varepsilon}(\omega)$. As we deal with driven harmonic oscillators as model systems in thin film optics (driving force =electromagnetic field, oscillation=polarization of the material), their differential equations have to be considered according to Ref. 28. They yield solutions in $\hat{\varepsilon}(\omega)$ and not in $\hat{n}(\omega)$. Thus the discussion will focus on the (imaginary part of the) complex dielectric function.

Anisotropic films, as it is the case here, require a more general treatment of the optical functions as tensors. Since our optical setup is characterized by nearly perpendicular incidence, we can only probe the z component (direction of the surface normal) of the complex dielectric tensor of organic films. In most applications of organic thin films these are indeed the components which matter. Moreover, what we want to demonstrate in this contribution is that the optical properties depend on the packing of the molecules, and this can be done concentrating on those z components.

The films we investigated exhibit two different kinds of anisotropy. As for the layer-by-layer grown films on HOPG (Sec. IV B), it is evident that they should fulfill the condition of uniaxial films since the substrate HOPG itself has no preferential long-range orientation. This gives rise to many azimuthally distributed HBC domains, though within one domain the growth is commensurate. As for the polycrystalline films on fused quartz (Sec. IV A), there is also no in-plane anisotropy at all since the crystallites are not oriented. However, there is a small anisotropy in the z direction, stemming from a slightly different volume fraction of the layers in this direction. As the total film thickness is very small and we have to treat the composite films (void+molecules) by an EMA model anyway (see Sec. IV D), this only adds a small uncertainty to our results.

We generally plotted optical density divided by energy (OD/E) versus energy to allow a direct comparison to ε''.[29] Despite this division by the energy, we will simply call these spectra "absorbance" or "optical density" in the following because the deviations from the optical density (as published in the literature) are hardly visible in this energy range.

III. EXPERIMENT

Our UHV system is equipped with electrically heated Knudsen-type effusion cells (K-cells) filled with organic molecules. For HBC, we obtained an evaporation rate of 1/8 of a monolayer[30] per minute at a temperature of about 425 °C inside the K-cell.[31] Because of the low base pressure of about 3×10^{-10} mbar and the resulting large mean free path, the sublimed molecules flow in a quite directed beam toward the sample.[32] The latter is held in a five-axial manipulator $(x, y, z, \vartheta, \varphi)$ equipped with a filament allowing one to heat the sample up to 800 °C.

The substrates were prepared under ambient conditions. Quartz glass substrates were cleaned in Extran and isopropanol ultrasonic baths. HOPG was cleaved along the basal planes using adhesive tape, producing atomically flat terraces. All substrates were degassed in UHV at 300 °C (200 °C for HOPG) for 1 to 2 h to remove water and other contaminants. Spectra were recorded at room temperature. Generally, fast Fourier transform (FFT) smoothing was applied to enhance the convergence of the numerical fit-procedure described briefly in Sec. II B.

All optical components are designed such that they reflect and transmit the ultraviolet-visible-near infrared light with little color aberration. Moreover, the lenses and windows mounted in and on the growth chamber are UHV-suitable, i.e., bakeable up to 250 °C. Our light source is a xenon arc lamp providing reasonably intense continuous light in the spectral range of 0.5–4 eV. For fast spectra recording, we use a commercially available optical multichannel analyzer consisting of a grating-mirror spectrograph (Acton Research SpectraPro-150, 300 g/mm blazed grating) followed by a back-illuminated charge-coupled device (Roper Scientific, SpectruMM 250B). The latter is single stage Peltier-cooled down to −35 °C which leaves a dark noise in the order of ≈0.5% per single spectrum. The attached 16 bit A/D converter

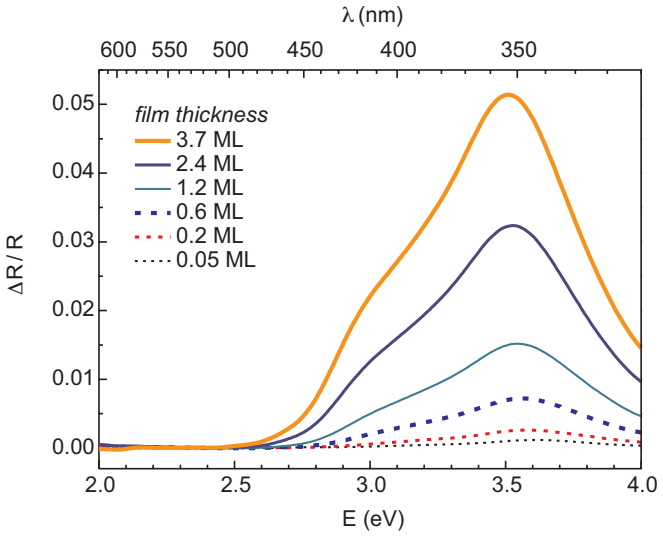

FIG. 3. (Color online) Drift-corrected *in situ* DRS series of HBC on fused quartz. Film thicknesses are given in equivalent units of surface coverage, 1 ML=1 monolayer.

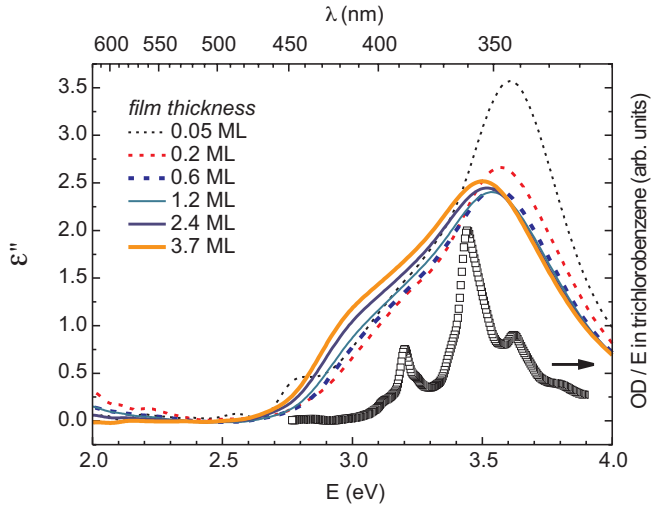

FIG. 4. (Color online) Thickness-dependent optical functions of HBC on fused quartz, calculated from the DRS shown in Fig. 3. In fact, the thickness-dependence of the spectra is quite low so that we only observe little changes in shape and magnitude of ε''. For comparison, the optical density of HBC in trichlorobenzene is drawn on a separate scale (open squares, cf. Fig. 2).

(100 kHz sampling rate) operates at 2^{16} counts per channel at best, which causes a statistical error of $\Delta N/N=N^{-1/2} \geqslant 0.4\%$, even for large-signal operation. Given that the investigated ultrathin layers only generate small changes in the reflection, an improvement of the signal-to-noise ratio is indispensable. This is achieved by the accumulation of typically 900–1800 successive acquisitions, leading to measuring times of 25–50 s which is short enough to carry out real-time measurements during film growth. Of course, then the recorded spectra represent a layer thickness range rather than a single thickness. The *in situ* optical setup is described in Ref. 6 in greater detail.

To account for spectral drift, we record the DRS under stable conditions immediately before and after the deposition of the molecules. The magnitude of the drift signal (over a broad energy range) is within 0.003 after 10 min while the "real" DRS signal during evaporation typically reaches maximum magnitudes of 0.02 in that time span. One finds a drift-induced relative error of 15% which is desired to be minimized. In most cases the drift can be approximated (in the spectral region of interest) by low-order polynomials whose coefficients show a monotonic development in time. The interpolation of these coefficients for the time between the two drift recordings leads to an estimation of the influence of the drift on the DRS spectra which can therefore be corrected subsequently.[25]

IV. RESULTS AND DISCUSSION

A. HBC on fused quartz

Fused quartz, which is sometimes called fused silica (SiO_2), is an amorphous glass. It usually has a low amount of impurities and is highly transparent down to wavelengths of approximately 170 nm. The latter attribute allows a direct interpretation of the DRS as being proportional to the absorbance (cf. Sec. II A). The *in situ* DRS series of HBC on fused quartz is shown in Fig. 3. According to Eq. (2), the DRS signal is proportional to the film thickness. Because the simple growth of the DRS signal with rising film thickness dominates this series, the spectral development is best viewed in the extracted ε'' data. As mentioned, this also facilitates the comparison of the optical functions on different substrates.

Figure 4 shows the imaginary part of the dielectric function calculated from the DRS measurements using the algorithm introduced in Sec. II B. Already at very low surface coverages of 0.05 ML the spectra show more resemblance to the absorbance spectrum of the bulk film than to the monomer absorbance in solution. The spectral shape converges very rapidly to the bulk behavior which is substantially reached at a nominal thickness of 0.2 ML. This behavior is due to a strong tendency of the HBC film to grow as three-dimensional islands. It is anticipated that the intermolecular interactions dominate the molecule-substrate interactions with the inert quartz glass. From Fig. 5 it is clear that HBC films on fused quartz are polycrystalline. The crystallites presumably exhibit the well-known bulk crystal structure of HBC (Ref. 19) [Fig. 1(a)] and have a typical diameter of 100 nm. The film growth is accompanied by a redshift of the main peak from 3.60 to 3.51 eV due to aggregation and intermolecular interaction. Additionally, a rather broad shoulder develops at around 3.0 eV with increasing film thickness. The features below 2.5 eV are most likely artifacts which could be due to drift effects. *Ex situ* absorbance measurements[21] clearly show that the optical density of HBC bulk structures on fused quartz vanishes for energies below 2.5 eV. As already mentioned, the curves are all noticeably broadened compared to the solution spectra of HBC.[12] Apart from the solvent shift, the absorbance spectrum of HBC in 1,2,4-trichlorobenzene is still different in shape compared to the ε'' spectra of the submonolayers. The main difference is

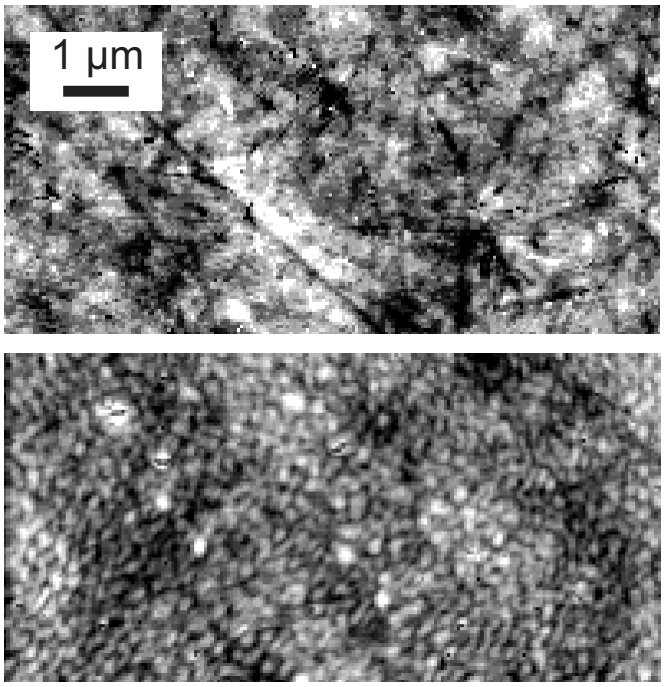

FIG. 5. AFM (TopoMetrix) topography images of bare fused quartz (upper half) and of a nominally 2.4 nm thick HBC film on fused quartz (lower half). The HBC film is polycrystalline with molecular islands of up to a few hundred nanometers in diameter. The height scale is 6 nm.

the visibility of sharp, distinct peaks (fine structure) of the isolated molecules in solution. Thus we cannot speak of monomers in the HBC film on quartz glass, even for a comparatively low number of molecules on the substrate.

B. HBC on HOPG

The layered structure of graphite and highly oriented pyrolytic graphite (HOPG) is well-known. In principle, it is a stack of widely expanded sheets of sp^2-hybridized carbon atoms. According to Ref. 33, the optical functions of graphite and HOPG coincide within experimental accuracy. Therefore, we will not consequently distinguish between both terms in the following.

From STM images,[34,35] LEED measurements,[36] and potential energy calculations[37] it is known that HBC forms highly ordered, densely packed monolayers on HOPG wherein the molecules are arranged flat on the surface. A combined study of atomic force microscopy, x-ray absorption spectroscopy, and photoelectron spectroscopy similarly reveals flat molecular terraces grown in a layer-by-layer fashion, even for 10 nm thick HBC-films on HOPG.[38] There, the authors point out that "strong [intermolecular] interactions lead to the formation of HBC stacks in which the molecular planes lie parallel to the surfaces of layered substrates" (HOPG). Likewise, Ruffieux *et al.* report the formation of columnar stacks (with small lateral offsets in the stacking direction but the molecular planes still being parallel to the substrate) of up to 3 ML HBC on Cu(111) and Au(111), evidenced by x-ray photoelectron diffraction and LEED.[39] The nearest neighbor distance between adjacent stacks is in the order of 14 to15 Å. A similar surface-induced vertical alignment of HBC on $MoS_2(0001)$ was found by Friedlein *et al.*[40] They observed quasi-one-dimensional structures by means of angle-resolved photoelectron spectroscopy. Jäckel *et al.* also speak of "nanographene stacks" on HOPG although their second monolayer of HBC is not as densely packed as the first one.[35] Yet, their STM study was carried out at the solid-liquid interface between HOPG and dissolved molecules, reducing the comparability to our experiments. All those experiments indicate that, due to the influence of the rather strong-binding substrates, the formation of columnar motifs occurs, being completely different from the bulk crystal structure of HBC.[32] In many ways, this growth mode resembles the quasi-one-dimensional crystal structure of PTCDA.

In a PTCDA crystal, the in-plane intermolecular distance in the (102) crystal plane [in most OMBE experiments parallel to the substrate's surface, cf. Fig. 1(b)] is much higher ($\approx$12–15 Å) than the distance in the stacking direction[41] ($\approx$3.4 Å).[5] The π-π overlap in the stacking direction is much stronger, yielding higher intermolecular interaction than within the crystal planes parallel to the surface. Consequently, up to a surface coverage of roughly 1 ML the molecular film behaves optically as being composed of an ensemble of monomers. Upon the formation of the next layer, the number of dimers increases with the same rate as the monomers from the first monolayer decrease until the second layer is completed, and so forth. Such a molecular crystal is referred to as quasi-one-dimensional. The exciton-model of the quasi-one-dimensional crystal is well-understood and is able to explain the excitonic processes which cause the thickness-dependent changes in the optical properties of PTCDA crystals.[7,8,42]

The three-dimensional character of the HBC bulk crystal structure [Fig. 1(a)] would require a much more complicated treatment of these effects. Coupling between the stacks may occur which would cause a stronger delocalization of the excitons. To the best of our knowledge, no appropriate exciton model exists for the bulk HBC crystal structure so far.

Our investigations were fueled by the question whether we could find optical evidence for the different growth mode of HBC on HOPG (layer-by-layer) with respect to the well-known bulk crystal modification (observed on inert substrates). Interestingly, we could find resemblances to the optical behavior of PTCDA indicating a columnar (quasi-one-dimensional) stacking.

As can be seen in Fig. 6, a direct interpretation of the DRS on HOPG as absorbance is not possible. The application of the numerical algorithm introduced in Sec. II B is indispensable to make statements on the optical properties of the molecular film.

The extracted ε'' spectra of HBC on HOPG are depicted in Fig. 7. For clarity, the three phases indicated in Fig. 6 are displayed separately. At the end of phase A and phase B, the ε'' spectra remain almost constant for two to three recorded consecutive thicknesses (not all shown) before the spectral development changes direction.

In phase A, the main feature shifts from 3.41 to 3.36 eV with increasing film thickness. The shoulder grows rather

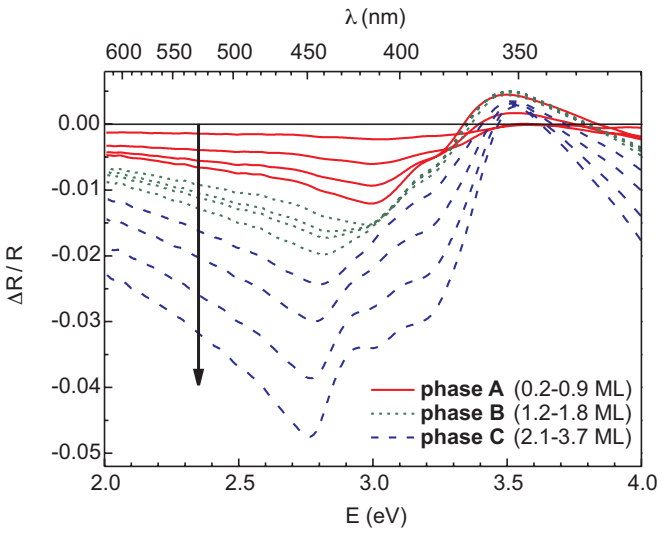

FIG. 6. (Color online) Drift-corrected *in situ* DRS series of HBC on HOPG. The arrow points in the direction of increasing film thickness. The series is divided into three phases. Solid lines: 0.2–0.9 ML (phase A), dotted lines: 1.2–1.8 ML (phase B), dashed lines: 2.1–3.7 ML (phase C).

constantly at 3.18 eV. Differently to quartz glass, HOPG possesses a high ability to interact with the HBC molecules because of the layered structure with π orbitals standing out of the graphite sheets. On fused quartz, we also observe broad spectra already from the beginning due to the formation of islands. Compared to that, intermolecular interactions are not necessarily the reason for the broadening on HOPG. HBC can actually be seen as a very small subunit of graphite, but saturated with hydrogen at the outermost carbon atoms. HBC and graphite have their π orbitals in common which are above and below the benzenoid framework. The parallel arrangement of the HBC molecules on the graphite sheets therefore allows an extensive π overlap and thus a rather strong molecule-substrate interaction. The main feature of the 0.2 ML spectrum happens to be at the same energy as the β-peak in solution (3.45 eV) coincidentally. The smaller features in solution at 3.20 eV (p-peak) and at 3.62 eV (β'-peak), however, correspond quite nicely to the shoulders observed in the broader submonolayer spectrum on HOPG. This can be checked by routinely performing Gaussian peak fits which are not shown here. Because of the rather good agreement of the submonolayer spectrum on HOPG with the solution spectrum we speak of broadened monomers on HOPG, at least their monomeric character is much more pronounced than on fused quartz. Below 2.8 eV there is an ensemble of peaks (or a broad feature) diminishing with increasing film thickness. Semiempirical calculations show that new transitions with varying intensity arise at energies below the main feature (β-peak) for charged HBC molecules. The calculations, based on semiempirical methods using configuration interaction (ZINDO/S, PM3), were done for free single molecules and not for solid molecular films. The accuracy of the calculations only permits the prediction of a downward shift in energy for charged molecules. However, a strong support for the assumption of charged molecules is the fact that the low energy features diminish for thicker layers.

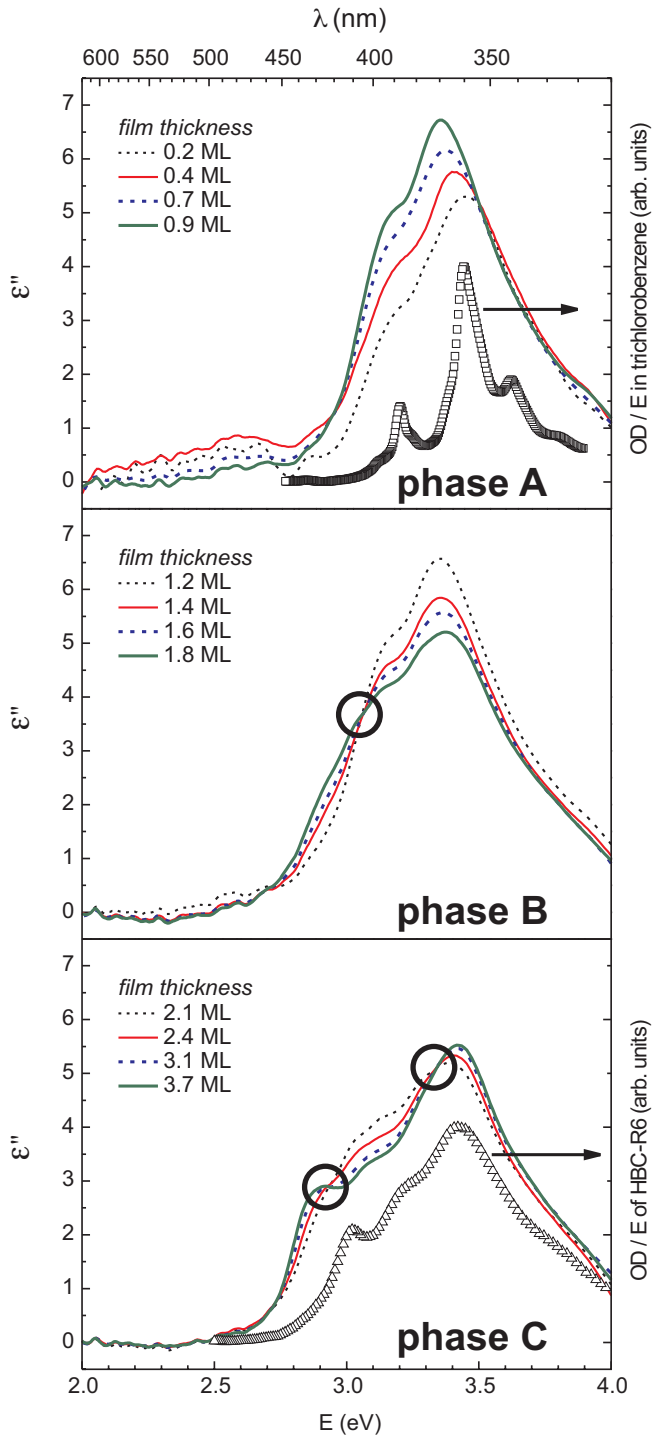

FIG. 7. (Color online) Thickness-dependent ε'' spectra of HBC on HOPG, calculated from the DRS shown in Fig. 6. The circles mark the visible isosbestic points. On HOPG, we generally observe ε'' values which are much higher than on fused quartz. This issue will be addressed in Sec. IV C. For comparison, the optical density of HBC in trichlorobenzene (open squares in phase A) and that of HBC-R6 aggregates (open triangles in phase C) are drawn on separate scales (cf. Fig. 2).

In phase B, the main peak at 3.36 eV and the shoulder at 3.18 eV reduce in strength whereas another shoulder at 2.9 eV begins to evolve. Consequently, an isosbestic point results at 3.08 eV indicating a physical reaction. With two

species $\mathcal{X}$ and $\mathcal{Y}$, an isosbestic point at a certain energy E_{ip} occurs when $\hat{\varepsilon}_{\mathcal{X}}(E_{ip})=\hat{\varepsilon}_{\mathcal{Y}}(E_{ip})$, and the sum of the concentrations of $\mathcal{X}$ and $\mathcal{Y}$ is constant. The physical reaction indicated by this first isosbestic point is the monomer→dimer transition. In a layer-by-layer structure, this occurs as soon as the first monolayer is filled and the second monolayer starts to grow. Hence the molecules begin to pile up into columnar stacks in this spectral series.

Finally, in phase C, the low energy shoulder at 2.9 eV continues to evolve and forms a small peak. The broad feature at around 3.1 eV further diminishes. The decrease of the main feature at 3.37 eV stops. It grows again very slightly, thereby moving to 3.42 eV. Two isosbestic points are visible, one at 2.94 eV and another one at 3.33 eV. Once more, it is anticipated that these isosbestic points are evidence for a physical reaction, in this case the dimer→oligomer[43] transition. The general shape of the final spectra of this series resembles quite nicely the absorbance spectrum of the columnar alkyl-substituted-HBC bulk structures on quartz glass. This is a strong hint to the formation of one-dimensional stacks on HOPG. The small spectral deviances are most likely due the lack of the alkyl-chains on the HBC molecules used here. Unsubstituted molecules certainly exhibit a slightly different packing behavior than the alkylated HBC and do provide a different dielectric background. Especially the fact that the spectrum of the 3.7 ML HBC film is broadened and its peaks are at slightly lower energies compared to HBC-R6 aggregates can be explained by the higher distance (and thus weaker excitonic coupling) of adjacent HBC-R6 stacks due to the steric hindrance introduced by the alkyl-chains.

Yet another major difference to the spectra on quartz glass is the occurrence of much higher ε'' values. This will be discussed in the next two sections in detail.

C. Oscillator strength

The oscillator strength f of an electronic transition (in solution) is more or less consistently defined in the literature.[44–46] Unfortunately, there is no trivial way to relate the oscillator strength in solution to that in a solid film. Assuming that the intermolecular distance in solution is rather large and no aggregates are formed, one can attribute the obtained value for f to single molecules. Contrary to that, the intermolecular interactions in a solid film already begin at low substrate coverages, as it is the case for HBC films on fused quartz. There, the early development of three-dimensional HBC islands most likely causes different optical transitions that must be attributed to the bulk (crystal-) structure.

The relative oscillator strength (OS) of the molecular films presented here is given by

$$\mathrm{OS} := \int_{\text{absorption band}} \varepsilon'' \times E dE. \tag{6}$$

This definition[47] stems from the "f-sum rules" that can be found in the literature.[48,49] If the ε'' spectrum of the submonolayers corresponds to the absorbance of the molecules in solution, one can principally find a conversion factor between OS and the value of f in solution. For HBC, no such factor could be found because of the lack of a clearly monomerlike spectrum on either substrate.

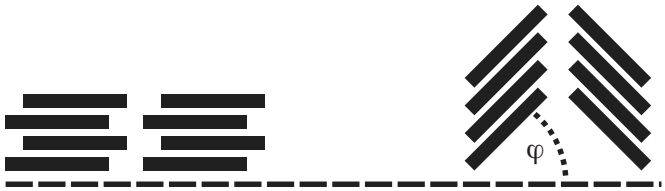

FIG. 8. Schematic visualization of the effect of a nonflat arrangement of HBC on the substrate. (left) Layer-by-layer growth and (right) crystal structure of HBC [side view, cf. Fig. 1(a)] at a certain angle φ.

First experiments show that the relative oscillator strength is not constant for increasing film thicknesses. In fact, it shows different tendencies on the substrates presented. Thus we will only compare the oscillator strength of the "bulk" structures, where the OS on either substrate converges to a constant value. This convergence meets our expectations because it has been shown that the bulk character of molecular layers is reached at film thicknesses of approximately 4 ML.[5,6] For HBC on the substrates presented, we extended the integral in Eq. (6) from 2.0 to 4.0 eV which covers the energetically lowest absorption band to a good approximation.

The magnitude of the oscillator strength of HBC on fused quartz ($\mathrm{OS}\approx 6.6\ \mathrm{eV}^2$) is remarkably lower than on HOPG ($\mathrm{OS}\approx 14\ \mathrm{eV}^2$). The factor of about 1/2 must be explained by the different film structures on these substrates. It was already mentioned that molecular growth on fused quartz is polycrystalline. A layer-by-layer growth can be excluded considering the evident differences to the shape of the ε'' spectra on HOPG. Thus the molecules do not lie flat on the quartz glass substrates but exhibit an angle φ between the molecular plane and the surface, cf. Fig. 8. Assuming that we have isotropically distributed molecules, the oscillator strength of HBC would be ≈82% of the value of flat lying molecules (for unpolarized light with an incident angle of 20° with respect to the surface normal). This estimation shows that the differences in the OS on the substrates presented cannot be exclusively explained by geometric arguments. Instead, morphology effects have to be considered as well.

D. Effective medium approximation

In order to account for effects of the film morphology, the effective medium approximation (EMA) is applied here. The simplest two-phase effective medium is sufficient to describe our situation of molecular structures "embedded" in void. There are several EMA models differing in the denotation of the host dielectric function $\hat{\varepsilon}_h$. The Bruggeman model[50] makes the self-consistent choice to assign the dielectric function of the host material to that of the total effective medium ($\hat{\varepsilon}_h=\hat{\varepsilon}_{\mathrm{eff}}$). In these terms, homogeneously distributed aggregates of small size are embedded in a host matrix whose optical behavior is determined by its composition of the two materials (molecules with $\hat{\varepsilon}_1$ and void with $\hat{\varepsilon}_2=1$). The cor-

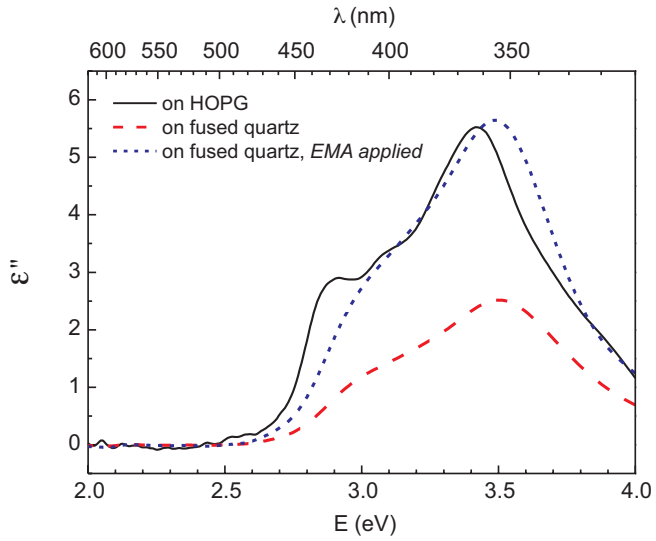

FIG. 9. (Color online) Comparison between the 3.7 ML ε'' spectra of HBC on HOPG (solid line) and on fused quartz [dashed line: raw data, dotted line: EMA applied using Eq. (7) with $f=0.60$].

responding equation for spherical enclosures is

$$0 = f\frac{\hat{\varepsilon}_1 - \hat{\varepsilon}_{\text{eff}}}{\hat{\varepsilon}_1 + 2\hat{\varepsilon}_{\text{eff}}} + (1-f)\frac{1-\hat{\varepsilon}_{\text{eff}}}{1+2\hat{\varepsilon}_{\text{eff}}}. \tag{7}$$

The volume fraction of the molecules in the entire layer is f. By means of Eq. (7), we can pass from the measured *effective* dielectric function $\hat{\varepsilon}_{\text{eff}}$ to the *intrinsic* dielectric function $\hat{\varepsilon}_{\text{int}} \equiv \hat{\varepsilon}_1$.

As an example, Fig. 9 depicts the application of Eq. (7) on the ε'' spectrum of a rough HBC film on fused quartz, in comparison to the closed film on HOPG. For both substrates, we have chosen the 3.7 ML spectra which already exhibit the properties of the respective bulk structures. The volume fraction of $f=0.60$ on fused quartz was chosen such that the resulting oscillator strength is 14 eV^2, which corresponds to the value of the same film thickness on HOPG. This volume fraction is in fairly good agreement to what the AFM pictures suggest. The main effect of reducing the volume fraction of the molecules is clearly an increase of the magnitude of $\hat{\varepsilon}_{\text{int}}$ (as compared to $\varepsilon''_{\text{eff}}$), and thus of the oscillator strength. Apart from that, spectral changes can hardly be noticed. The main peak shifts only very slightly from 3.50 to 3.49 eV upon dilution with void. Its counterpart on HOPG is at 3.42 eV. These peak positions are practically identical to the main peaks of the two bulk structures shown in Fig. 2. Likewise, the smaller peak of HBC on HOPG at around 2.9 eV only has an equivalent in the columnar HBC-R6 structures and *not* in the polycrystalline film on fused quartz.

V. SUMMARY AND CONCLUSIONS

We performed thickness-dependent optical investigations of HBC films deposited by means of organic molecular beam epitaxy (OMBE) on different substrates, namely fused quartz and HOPG. The highly sensitive differential reflectance spectroscopy (DRS) was employed *in situ*, i.e., during film growth. By means of a model-free numerical algorithm, we were able to extract the optical functions of the HBC films from the DRS measurements.

We found polycrystalline island growth on fused quartz, whereas highly ordered layer-by-layer growth on HOPG has previously been reported. Our obtained ε'' spectra of HBC films on fused quartz strikingly resemble *ex situ* recorded absorbance spectra of polycrystalline HBC bulk structures. In contrast, the presented optical spectra of HBC films on HOPG are in nice agreement with the absorbance of columnar HBC-R6 bulk structures. For HBC on HOPG, we observed a monomer→dimer→oligomer transition, indicated by the occurrence of isosbestic points in the ε'' spectra. This behavior is in analogy with the growth of quasi-one-dimensional PTCDA crystals on mica. Thus the growth of HBC crystals is significantly altered by the HOPG surface (substrate-induced growth).

Large varieties in the absolute values of the oscillator strength (OS) of HBC on the different substrates were found. The polycrystalline island films on fused quartz exhibit only about 1/2 of the OS of highly ordered closed films on HOPG. It was shown that this factor cannot be exclusively explained by geometrical arguments of the angular arrangement of the molecules with respect to the surface. Instead, an effective medium approximation (EMA) model was proposed. This EMA model accounts for the effects of rough molecular films and is able to give an answer to the observed discrepancies in the OS.

ACKNOWLEDGMENTS

One of the authors (R.F.) wishes to thank O. Mieth for providing assistance with the AFM images. Funding of this work by the "Deutsche Forschungsgemeinschaft" (DFG) via Grants No. FR 875/6 and FR 875/9 is gratefully acknowledged. We highly appreciate fruitful discussions and financial support by K. Leo (Le 747/31-1).

*Electronic address: fritz@iapp.de; URL: www.iapp.de

[1] C. W. Tang, Appl. Phys. Lett. **48**, 183 (1986).
[2] C. W. Tang and S. A. VanSlyke, Appl. Phys. Lett. **51**, 913 (1987).
[3] J. D. E. McIntyre and D. E. Aspnes, Surf. Sci. **24**, 417 (1971).
[4] S. Kim, Z. Wang, and D. A. Scherson, J. Phys. Chem. B **101**, 2735 (1997).
[5] H. Proehl, T. Dienel, R. Nitsche, and T. Fritz, Phys. Rev. Lett. **93**, 097403 (2004).
[6] H. Proehl, R. Nitsche, T. Dienel, K. Leo, and T. Fritz, Phys. Rev. B **71**, 165207 (2005).
[7] M. Hoffmann and Z. G. Soos, Phys. Rev. B **66**, 024305 (2002).
[8] M. Knupfer, T. Schwieger, J. Fink, K. Leo, and M. Hoffmann,

Phys. Rev. B **66**, 035208 (2002).
[9] M. Hoffmann, in *Electronic Excitations in Organic Multilayers and Organic Based Heterostructures*, edited by V. M. Agranovich and G. F. Bassani (Elsevier, Amsterdam, 2003), Vol. 31 of *Thin Films and Nanostructures*, Chap. 5, pp. 221–292.
[10] M. Leonhardt, O. Mager, and H. Port, Chem. Phys. Lett. **313**, 24 (1999).
[11] R. Nitsche and T. Fritz, Phys. Rev. B **70**, 195432 (2004).
[12] W. Hendel, Z. H. Khan, and W. Schmidt, Tetrahedron **42**, 1127 (1986).
[13] S. Ito, P. T. Herwig, T. Böhme, J. P. Rabe, W. Rettig, and K. Müllen, J. Am. Chem. Soc. **122**, 7698 (2000).
[14] M. G. Debije, J. Piris, M. P. de Haas, J. M. Warman, Ž. Tomović, C. D. Simpson, M. D. Watson, and K. Müllen, J. Am. Chem. Soc. **126**, 4641 (2004).
[15] J. Piris, M. G. Debije, N. Stutzmann, B. W. Laursen, W. Pisula, M. D. Watson, T. Bjornholm, K. Müllen, and J. M. Warman, Adv. Funct. Mater. **14**, 1053 (2004).
[16] Z. Wang, M. D. Watson, J. Wu, and K. Müllen, Chem. Commun. (Cambridge) 2004, 336.
[17] J. Wu, M. D. Watson, N. Tchebotareva, Z. Wang, and K. Müllen, J. Org. Chem. **69**, 8194 (2004).
[18] J. Wu, J. Qu, N. Tchebotareva, and K. Müllen, Tetrahedron Lett. **46**, 1565 (2005).
[19] R. Goddard, M. W. Haenel, W. C. Herndon, C. Krüger, and M. Zander, J. Am. Chem. Soc. **117**, 30 (1995).
[20] M. Möbus, N. Karl, and T. Kobayashi, , J. Cryst. Growth **116**, 495 (1992).
[21] H. Proehl, M. Toerker, F. Sellam, T. Fritz, K. Leo, C. Simpson, and K. Müllen, Phys. Rev. B **63**, 205409 (2001).
[22] E. Clar, C. T. Ironside, and M. Zander, J. Chem. Soc. 1959, 142.
[23] J. S. Toll, Phys. Rev. **104**, 1760 (1956).
[24] B. E. A. Saleh and M. C. Teich, *Fundamentals of Photonics* (Wiley, New York, 1991).
[25] R. Nitsche, Ph.D. thesis, TU Dresden, 2005.
[26] R. Forker, diploma thesis, TU Dresden, 2005.
[27] The relation between the complex refractive index $\hat{n}(\omega)=n(\omega)-ik(\omega)$ and the complex dielectric function $\hat{\varepsilon}(\omega)=\varepsilon'(\omega)-i\varepsilon''(\omega)$ is $\hat{\varepsilon}=\hat{n}^2=n^2-k^2-2ink$.
[28] L. D. Landau and E. M. Lifschitz, *Elektrodynamik der Kontinua* (Akademie-Verlag, Berlin, 1980).
[29] The optical density is given (after the Beer-Lambert law) by $OD=(4\pi/\lambda)kcd$, where k stems from the complex refractive index of the molecules in solution ($\hat{n}_{\text{molecules}}=n-ik$), c is the concentration and d the thickness of the cuvette. For weakly absorbing solvents and small concentrations, we can write $OD=(4\pi/\lambda)(\varepsilon''_{\text{molecules}}/2n_{\text{solvent}})cd$. Assuming n_{solvent} to be nearly constant for the solvents used in the Refs. 12 and 14, we can state that the optical density is proportional to ($\varepsilon''_{\text{molecules}}/\lambda$) or ($\varepsilon''_{\text{molecules}}\times E$). Thus, we have $OD/E\propto\varepsilon''_{\text{molecules}}$.
[30] One monolayer (ML) has a nominal thickness of about 0.32 nm.
[31] We systematically attempted to grow closed layers on different (conductive) substrates which were imaged by STM. The first monolayer was visible after 8 min, the second after roughly twice that time, confirming a rather constant growth rate. We assume equal sticking coefficients on the substrates presented.
[32] Hence the term organic molecular beam epitaxy (OMBE).
[33] *Handbook of Optical Constants of Solids II*, edited by E. D. Palik (Academic Press, New York, 1991).
[34] T. Schmitz-Hübsch, F. Sellam, R. Staub, M. Törker, T. Fritz, C. Kübel, K. Müllen, and K. Leo, Surf. Sci. **445**, 358 (2000).
[35] F. Jäckel, M. D. Watson, K. Müllen, and J. P. Rabe, Phys. Rev. B **73**, 045423 (2006).
[36] U. Zimmermann and N. Karl, Surf. Sci. **268**, 296 (1992).
[37] S. Mannsfeld, Ph.D. thesis, TU Dresden, 2004.
[38] M. Keil, P. Samorí, D. A. dos Santos, T. Kugler, S. Stafström, J. D. Brand, K. Müllen, J. L. Brédas, J. P. Rabe, and W. R. Salaneck, J. Phys. Chem. B **104**, 3967 (2000).
[39] P. Ruffieux, O. Gröning, M. Bielmann, C. Simpson, K. Müllen, L. Schlapbach, and P. Gröning, Phys. Rev. B **66**, 073409 (2002).
[40] R. Friedlein, X. Crispin, C. D. Simpson, M. D. Watson, F. Jäckel, W. Osikowicz, S. Marciniak, M. P. de Jong, P. Samorí, S. K. M. Jönsson, M. Fahlman, K. Müllen, J.P. Rabe, and W. R. Salaneck, Phys. Rev. B **68**, 195414 (2003).
[41] The stacking direction is not exactly perpendicular to the (102) crystal plane in which the molecules lie flat. Thus the separation of two adjacent (102) planes is slightly lower than the given intermolecular distance in the stacking direction.
[42] M. Hoffmann, Z. G. Soos, and K. Leo, Nonlinear Opt. **29**, 227 (2002).
[43] It is not uniquely the dimer→trimer transition because the isosbestic points are visible up to ≈4 monolayers.
[44] H. Suzuki, *Electronic Absorption Spectra and Geometry of Organic Molecules* (Academic Press, New York, 1967).
[45] J. B. Birks, *Photophysics of Aromatic Molecules* (Wiley-Interscience, London, 1970).
[46] M. Pope and C. E. Swenberg, *Electronic Processes in Organic Crystals* (Oxford University Press, New York, 1982).
[47] This is only a proportionality as we have dropped some factors of the actual definition of the f-sum rules.
[48] M. Altarelli, D. L. Dexter, H. M. Nussenzveig, and D. Y. Smith, Phys. Rev. B **6**, 4502 (1972).
[49] D. Stroud, Phys. Rev. B **19**, 1783 (1979).
[50] D. A. G. Bruggeman, Ann. Phys. (Paris) **5**, 636 (1935).